Effect of iodine incorporation on characteristic properties of cadmium telluride deposited in aqueous solution

OJO, A. A. and DHARMADASA, I <http://orcid.org/0000-0001-7988-669X>

Effect of Iodine Incorporation on Characteristic Properties of Cadmium Telluride Deposited in Aqueous Solution.

A. A. Ojo* and I. M. Dharmadasa

Electronic Materials and Sensors Group, Materials and Engineering Research Institute (MERI), Sheffield Hallam University, Sheffield S1 1WB, UK.

*Email: chartell2006@yahoo.com; Tel: +44 114 225 6910 Fax: +44 114 225 6930

Abstract

The electrodeposition of polycrystalline I-doped CdTe was successfully performed from aqueous solutions containing cadmium nitrate ($Cd(NO_3)_2$ and tellurium oxide (TeO_2). The effects of different I-doping concentrations in the electrolytic bath on the deposited CdTe layers deposited were evaluated structurally, optically, morphologically and electronically using X-ray diffraction (XRD), ultraviolet-visible spectrophotometry, scanning electron microscopy, photoelectrochemical cell measurement and direct-current (DC) conductivity test respectively. The XRD show reduction in the (111) cubic CdTe peak intensity and the calculated crystallite size of the CdTe:I layers above 5 ppm I-doping. At I-doping of 1000 ppm of the CdTe-bath and above, the deposition of only crystalline Te due to the formation of Cd-I complexes debarring the deposition of Cd and co-deposition of CdTe in aqueous solution was observed. Morphologically, reductions in grain size were observed above 5 ppm I-doping with high pinhole density and the formation of cracks within the CdTe:I layers. For the as-deposited CdTe:I layers, conduction type remained *n*-type across all the explored I-doping concentration of 200 ppm. For the $CdCl_2$ and $Ga_2(SO_4)_2$+$CdCl_2$ treated CdTe:I layers, the transition from *n*- to *p*-type conductivity was observed for the CdTe:I baths doped with 20 ppm and above due to the reduced cadmium deposition on the substrate. The highest conductivity was observed at 5 ppm I-doping of the CdTe-bath. Observations made on the CdTe:I in aqueous solution differs from the non-aqueous solvent documented in the literature. These results are reported systematically in this communication.

Keyword: Electrodeposition; cadmium telluride; thin films; doping; iodine

1 Introduction

The use of II-VI semiconductors such as cadmium telluride (CdTe) has attained eminence decades ago due to its material and electronic properties [1]. As compared to other semiconductors (SC) of cadmium chalcogenides, CdTe does possess advantages such as comparatively high mobility, conductivity type tuning based on the elemental composition of Cd and Te, photosensitivity amongst other attributes. Therefore, CdTe has been well explored and utilised in applications such as crystal diodes, transistors, radiation detectors, photodiodes and photovoltaic cells among others. With emphasis on application specific property such as photovoltaic, CdTe has a near ideal bandgap of 1.45 eV [1] as first demonstrated theoretically by Loferski [2] and afterward by Shockley et al [3] using a single *p-n* junction model. They demonstrated that comparatively low current density and high potential barriers can be generated from high bandgap photovoltaic materials, while in the lower bandgap photovoltaic materials, the reverse is the case for the obtainable current density and potential barriers. The single *p-n* junction incorporating *p*-CdTe as the absorber layer has been the norm while CdS which is intrinsically doped *n*-type due to sulphur vacancy and cadmium interstitials [4,5] have been mostly utilised due to their relatively low lattice mismatch of ~10% [6,7]. Based on new understanding as documented in the literature [8,9], barrier heights larger than 0.90 eV are achievable by utilising suitable *n*-CdTe layers. This new understanding is further to the literature as documented in 1998 by Dharmadasa [10] with the association of defect level E1 (0.40 eV), E2 (0.65 eV) and E3 (0.730 eV) with Te richness in CdTe while E4 (0.96 eV) and E5 (1.18 eV) are associated with Cd richness in CdTe in which higher barrier heights up to 1.20 eV can be achieved. Although Cd-rich CdTe can be achieved intrinsically, this work focuses on the optimisation of extrinsic iodine doping of CdTe since it is the best atomic replacement for Te atom with minimal deformation to the CdTe lattice. Both Te and I have an atomic radius of 1.4×10^{-10} m.

2 Experimental details

2.1 Electrolytic bath preparation

All the chemicals and the transparent conducting substrates utilised in the work were procured from Sigma Aldrich. The electrolytic baths from which CdTe:I layers were electroplated contained 1.5 M cadmium nitrate ($Cd(NO_3)_2$) with a purity of 99.997% and 0.0002 M of tellurium dioxide with a purity of 99.995% in 400 ml of deionised (DI) water. Varying concentration of cadmium iodide (CdI_2) with a purity of 99.999% was added to the CdTe electrolyte to Iodine-doping concentrations between 0 ppm and 200 ppm. The overall ~400 ml

aqueous solutions were contained in 500 ml polypropylene plastic beakers and housed in 1000 ml glass beakers. Low quantity of water is contained in the glass beaker to achieve uniformity in heating the electrolyte contained in the polypropylene beaker. The iodine-doped electrolytic baths were stirred for at least 5 h to achieve homogeneity before CdTe:I deposition. In addition, the stirring rate, bath temperature and pH of the electrolytic were adjusted to ~300 rpm, 85°C and 2.00±0.02 respectively prior to CdTe:I deposition. A high purity graphite rod was utilised as the anode while the transparent conducting substrate (glass/fluorine doped tin oxide (FTO)) was the cathode. Based on prior experimentation and optimisation of CdTe layer deposited from pure $Cd(NO_3)_2$ bath as described in Ref. [11], all the CdTe:I layers in these sets of experiment were deposited at 1400 mV for 2 h.

2.2 Substrate preparation

TEC7 glass/FTO substrates with a sheet resistance of 7 Ω/sq were utilised for this sets of experiments. The substrates were cut into 3×3 cm^2 dimension, washed in an ultrasonic bath containing soap solution, rinsed in DI water and degreased using both methanol and acetone solutions. Finally, the substrates were rinsed in DI water and transferred directly into the electrolyte as the cathode.

2.3 Post-growth treatment

After electroplating the CdTe:I layers from respective electrolytic baths containing different I-doping concentrations, the glass/FTO/CdTe:I layers were rinsed in DI water, cut into 3 pieces of 1×3 cm^2 dimensions each and dried in a stream of nitrogen gas. From each of the CdTe:I samples with different I-doping concentration cut into 3 pieces each, one is left as-deposited (AD), while the other two were dipped into aqueous solutions containing 0.1 M cadmium chloride ($CdCl_2$) only solution or a mixture of 0.05 M gallium sulphate ($Ga_2(SO_4)_3$) plus 0.1 M $CdCl_2$ respectively for 5 sec and allowed to air-dry. Afterward, both the $CdCl_2$ treated and the $Ga_2(SO_4)_3$ + $CdCl_2$ treated samples which will be referred to as CCT and GCT were heat-treated at 420°C for 20 min in air to improve both the material and electronic properties of CdTe layer [12,13]. All the glass/FTO/CdTe:I layers were explored analytically to determine the effect of I-doping concentration in CdTe bath and its effect on the post-growth treated layers.

2.4 Experimental techniques used

Information about phase identification, crystallite size, preferred orientation of the electroplated CdTe:I layers were acquired using Philips PW 3,710 X'pert diffractometer with

Cu-Kα monochromator of wavelength λ = 1.54 Å. For these sets of experiments, the X-ray tension was set to 40 kV while the current was set to 40 mA, while the diffractions were recorded between the 2θ angle of 20° and 70°. The optical properties were obtained using Cary 50 Scan UV–Vis spectrophotometer at room temperature within the wavelength range was set between 200 nm and 1000 nm. Prior to optical measurements, the baseline was set using blank glass/FTO to isolate the effects of glass/FTO on the optical properties of the deposited CdTe:I layer. Using FEI Nova 200 NanoSEM at a chamber pressure of ~1.99×10^{-2} Nm^{-2} and magnification of ×60,000 details on both the morphological and compositional properties of the CdTe:I layer were obtained. The scanning electron microscopy (SEM) equipment utilised (FEI Nova 200 NanoSEM) contains an Energy-dispersive X- ray spectroscopy (EDX) compartment. The conductivity type of the CdTe:I layers were obtained using photoelectrochemical (PEC) cell measurement. This was performed by forming a solid/liquid junction between the glass/FTO/CdTe:I layer and 0.1 M $Na_2S_2O_3$ aqueous solution. The voltage difference between measurements taken under illuminated condition (V_L) and under dark condition (V_D) at constant time interval signifies both the conductivity type and the suitability of doping concentration of the semiconducting layer for fabricating electronic devices [14]. Other electrical properties such as the DC conductivity measurement of the CdTe:I layers were performed using Rera solution fully automated I–V measurement system.

3 Result and discussion

3.1 X-ray diffraction analysis

Figure 1 (a-c) shows the X-ray diffraction (XRD) spectra of CdTe:I layers under AD, CCT and GCT conditions grown from electrolytic baths containing different I-concentration respectively. Figure 1 (d) shows the CdTe (111) cubic intensity at different post-growth treatment against I-doping concentration in the CdTe electrolytic bath.

From observation, diffraction peak associated with CdTe (111), (220) and (311) all in the cubic phase were observed asides from the diffractions associated with the glass/FTO underlying substrates. It should be noted that the extracted XRD data from these CdTe:I work matches the Joint Committee on Powder Diffraction Standards (JCPDS) reference file number 01-075-2086 on cubic CdTe layers. From observations in Figure 1 (a-c), diffractions associated with elemental iodine or iodine related compounds were not observed in all of the explored XRD layers, which might be due to the low concentrations explored and the sensitivity of the XRD technique. Under all treatment conditions, CdTe (111) diffraction shows the highest diffraction

intensity which is synonymous with the preferred orientation of CdTe:I layer under the growth conditions of this study.

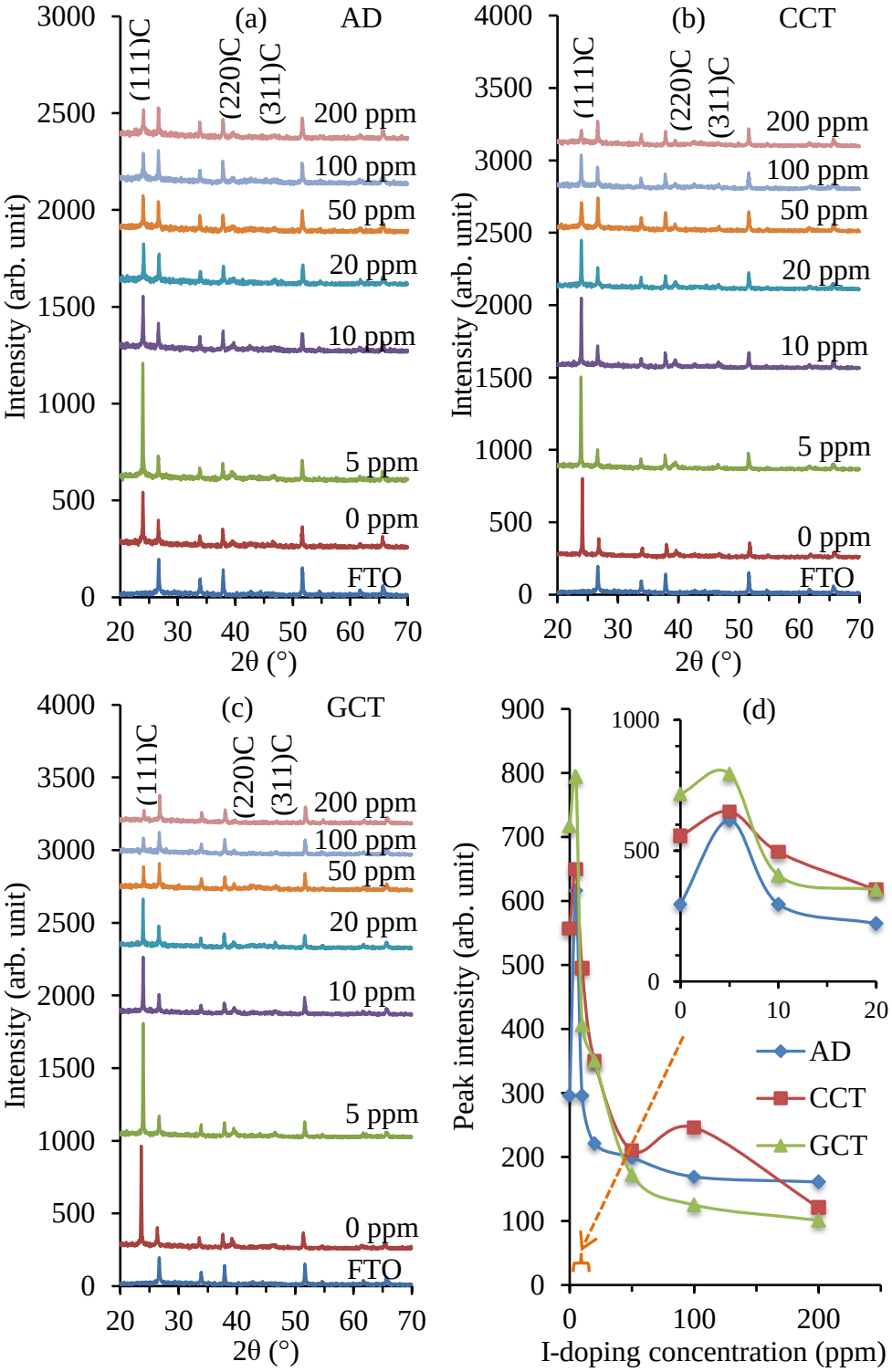

Figure 1: Typical XRD patterns of CdTe:I at different iodine doping concentrations for (a) AD (b) CCT and (c) GCT, while (d) is the graph of (111) CdTe peak intensity against I-doping concentration. (The inset is the expanded 0 to 20 ppm I-doping of the CdTe bath)

Comparative improvement in the CdTe:I layers were observed after CCT or GCT as shown by higher (111)C CdTe XRD intensity as compared to the AD CdTe:I layers. This observation can be attributed to Cd/Te stoichiometric improvement by sublimation of excess elements or the formation CdTe by the reaction between excess elemental Te and Cd from $CdCl_2$ treatment [7]. As shown in Figure 1 (a-c), under AD, CCT and GCT conditions an initial increase in the (111) cubic CdTe diffraction intensity was observed from 0 ppm to 5 ppm I-doping which signifies an improvement in the CdTe:I crystallinity, while a gradual decline in the diffraction intensity of CdTe:I were observed at I-doping concentration at 10 ppm and above as clearly shown in Figure 1 (d). The observed reduction in X-ray diffraction intensity of the (111)C peak at ~5 ppm I-doping and above might be due to the deterioration of CdTe layer affected reduced free Cd ions in the formation of CdTe. This reduction is due to the formation of Cd-I complexes such as CdI^+, CdI_2, CdI_3^- and CdI_4^{2-} in aqueous solution [15,16] and as documented in the literature, highest crystallinity of CdTe is achievable with 1:1 atomic ratio of Cd to Te [17,18]. However, the formation of Cd-I complexes are formed only in aqueous solution and not effective in the non-aqueous electrolytic deposition of CdTe incorporating iodine [19].

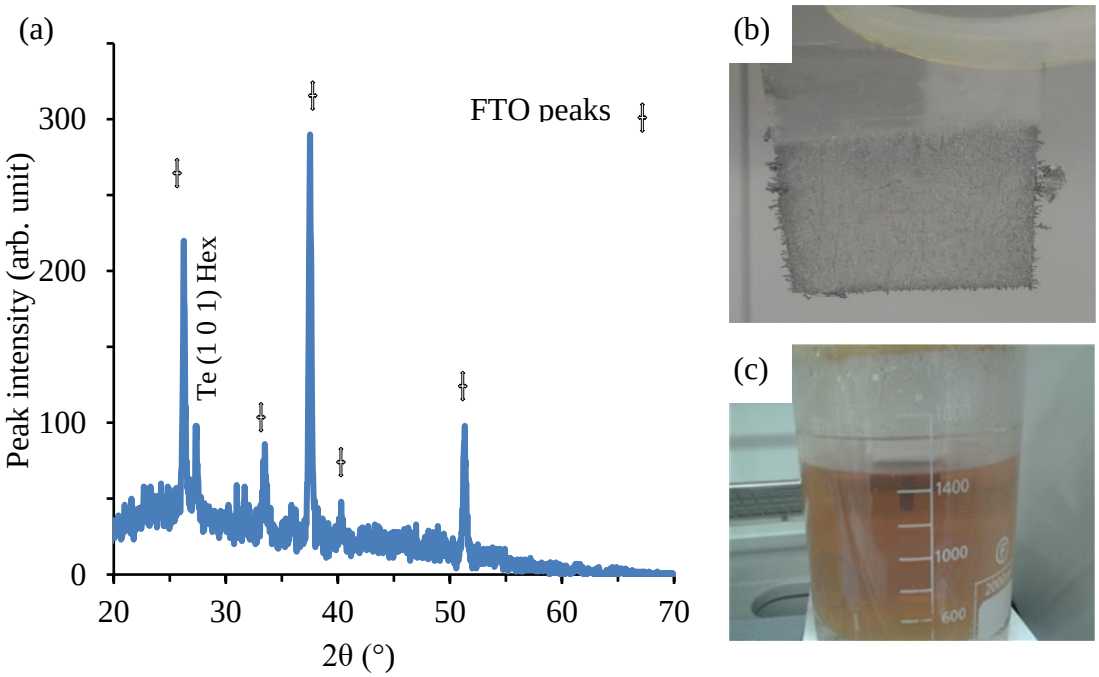

Figure 2: (a) Typical XRD pattern of Te grown at 1000 ppm I-doping of CdTe, (b) deposited Te layer and (c) unstable CdTe bath with 1000 ppm I-doping.

The complexes Cd-I formed hinder the deposition of Cd^{2+} ions on the surface of the working electrode and also the reduces the available Cd^{2+} with increasing CdI_2 concentration as suggested by Paterson et al [15,16]. Therefore, the CdTe layers deteriorate due to lack of Cd in the deposited film [17]. The explored I-doping concentration range was limited to 200 ppm due to a further reduction in the cubic (111) CdTe intensity (without re-crystallisation) and total elimination at ~1000 ppm with the appearance of the emergence of the Hex (101) Te peak as shown in Figure 2. This observation signifies the non-deposition of Cd on the glass/FTO substrate at high I-doping concentration.

Table 1: Summary of the X-ray diffraction analysis for cubic (111) CdTe diffraction.

AD				
Doping (ppm)	2θ (°)	d-spacing (Å)	FWHM (°)	Crystallite size (nm)
0	23.92	3.716	0.129	65.4
5	23.91	3.718	0.129	65.4
10	23.97	3.709	0.129	65.4
20	23.98	3.708	0.129	65.4
50	23.97	3.709	0.162	52.3
100	24.06	3.695	0.162	52.3
200	24.03	3.699	0.162	52.3
CCT				
Doping (ppm)	2θ (°)	d-spacing (Å)	FWHM (°)	Crystallite size (nm)
0	23.94	3.713	0.129	65.4
5	24.11	3.688	0.129	65.4
10	23.89	3.72	0.162	52.3
20	23.95	3.713	0.162	52.3
50	23.94	3.714	0.162	52.3
100	23.95	3.712	0.162	52.3
200	23.95	3.712	0.259	32.7
GCT				
Doping (ppm)	2θ (°)	d-spacing (Å)	FWHM (°)	Crystallite size (nm)
0	23.9	3.720	0.129	65.4
5	23.99	3.706	0.129	65.4
10	24.07	3.694	0.129	65.4
20	23.6	3.767	0.162	52.3
50	23.92	3.717	0.162	52.3
100	23.98	3.708	0.162	52.3
200	23.92	3.717	0.162	52.3

Table 1 shows the cubic (111) CdTe X-ray diffraction analysis for AD, CCT and GCT CdTe:I layers. The crystallite sizes were calculated using Scherrer equation as shown in equation (1), where D is the crystallite size, λ is the wavelength of the X-rays used (1.542 Å), β is the full width at half maximum (FWHM) of the diffraction peak calculated in radian and θ is the Bragg angle.

$$D = \frac{0.94\lambda}{\beta \cos\theta} \tag{1}$$

For the as-deposited CdTe:I layer as shown in Table 1, a gradual reduction in the d-spacing was observed with increase in I-doping concentrations, while CdTe:I samples with concentrations above 100 ppm exhibit a major alteration in the d-spacing. This observation iterates the presence of tensile stress in the crystal plane due to the introduction of I-doping. Under AD conditions, a constant crystallite of 65.4 nm was observed for CdTe:I doped layer with I-doping concentration ranging between 0 ppm and 20 ppm. Above this range, the crystallite size was reduced to ~52.3 nm. Similar trends of reduction in the crystallite sizes were observed under the CCT above 5 ppm I-doping and GCT above 10 ppm I-doping concentration. Although, alteration in crystallite stress distribution, compositional configuration, oxidation and grain growth amongst other factors may drastically affect the crystallite parameters as observed in Table 1. It should be noted that the stagnated crystallite sizes at 65.4 nm and 52.3 nm might be due to the limitation of the use of the Scherrer's equation for materials with larger grains as well as the XRD machine [20,21].

3.2 Optical properties analysis

The optical absorbance of the CdTe:I under AD, CCT and GCT conditions were performed at room temperature. The bandgap of the CdTe:I layers were determined using Tauc's plot of $(\alpha h\nu)^{1/m}$ against photon energy ($h\nu$) where ν is the frequency of electromagnetic radiation, h is the planks constant, α is the absorption coefficient of CdTe and m is the power factor of the transition mode. The value m equals 0.5 for direct bandgap and 2 for indirect bandgap materials [22]. Figure 3 (a-c) show the Tauc's plot of AD, CCT and GCT CdTe:I at different I-doping concentrations respectively. While Figure 3 (d) shows a graph of absorption edge slope against I-doping concentrations of CdTe baths and Table 2 shows the optical absorption properties of the CdTe:I layers under all the conditions explored in this work. From observation, all the explored I-doping concentration from 0 ppm to 200 ppm falls within the range of 1.52±0.05 eV for the AD CdTe:I layers with increase in the I-doping concentration resulting into increase in the bandgap, while both the CCT and GCT layers falls within the range of 1.48±0.01 eV and

1.47±0.02 eV respectively. The improvement towards the acceptable CdTe bandgap range of 1.44 eV and 1.50 eV [23] and the narrowing of the bandgap range is due to the enhancement of material properties such as grain growth, crystallinity, removal of defects and sublimation of excess element [7,24,25] amongst others.

Furthermore, the optical absorption edge slope which is a quantitative measure of defect and impurity energy levels [7,26] were explored as a function of I-doping concentration as shown in Figure 3 (d). Under all the post-growth treatment conditions explored in this work, the highest absorption edge slope was observed at 5 ppm I-doping concentration.

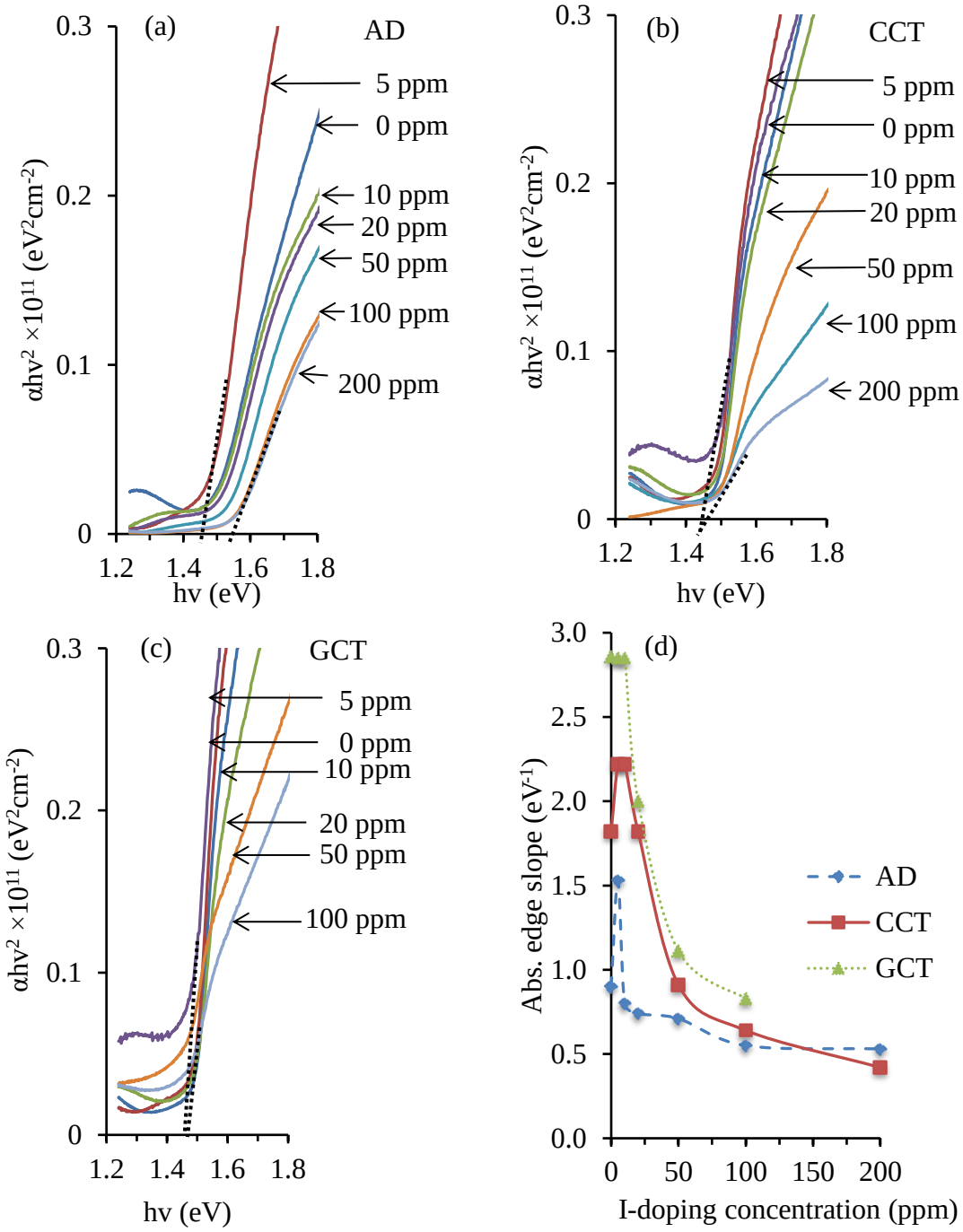

Figure 3: Optical absorption of CdTe:I with different doping concentrations of iodine under (a) AD, (b) CCT and (c) GCT conditions, while (d) is the absorption edge slope of CdTe:Ga under AD, CCT and GCT conditions against I-doping concentration.

This comparatively signifies that more incident photons can be absorbed in few micron thickness of CdTe:I and also increased possibility of achieving higher solar to electricity conversion efficiency when incorporated in solar cell structures.

Table 2: The optical bandgap and slope of absorption edge of CdTe layers grown from different CdTe baths with different I-doping concentrations and undergone different post-growth treatments.

I-doping (ppm)	Bandgap (eV)			Abs. edge slope (eV^{-1})		
	AD	CCT	GCT	AD	CCT	GCT
0	1.47	1.47	1.46	0.90	1.82	2.86
5	1.47	1.48	1.49	1.53	2.22	2.85
10	1.49	1.49	1.49	0.80	2.22	2.85
20	1.50	1.49	1.48	0.74	1.82	2.00
50	1.53	1.49	1.45	0.71	0.91	1.11
100	1.55	1.49	1.45	0.55	0.64	0.83
200	1.56	1.49		0.53	0.42	

3.3 Morphological and compositional property analysis

Figure 4 shows the SEM micrographs of CdTe:I incorporating (a) 5 ppm I-doping under CCT and (b) under GCT, while (c) incorporating 100 ppm I-doping under CCT and (d) under GCT. The as-deposited CdTe:I and 0 ppm I-doped CdTe layers were not incorporated due to its triviality.

In accord with the effect of CCT and GCT as documented in the literature, grain growths were observable as compared to the as-deposited CdTe:I layers. Comparatively, a reduction in the grain size was observed above 5 ppm I-doping of the CdTe bath which may be due to competing phases of Cd-I complexes in aqueous solution as suggested in the literature [15,16]. This observation is corroborative with the structural and optical analytical observations.

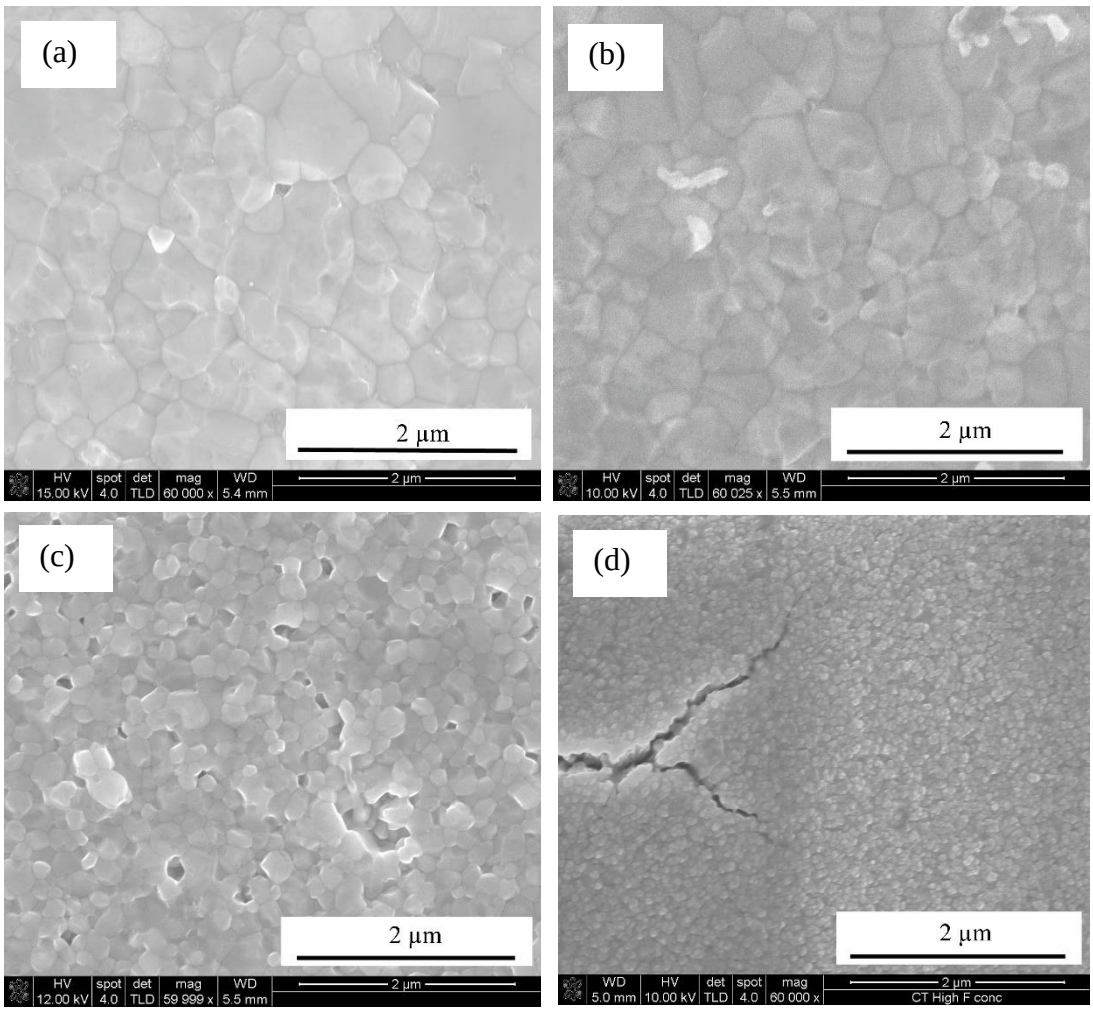

Figure 4: Typical SEM micrographs of CdTe:I (a) incorporating 5 ppm I-doping under CCT and (b) under GCT, while (c) incorporating 100 ppm I-doping under CCT and (d) under GCT.

Figure 5 (a-c) shows the compositional analysis of both the CCT and the GCT treated CdTe layers using EDX spectra of individual CdTe samples grown at 0, 5 and 20 ppm I-doping in the CdTe-bath respectively. Figure 5 (d) shows the compositional analysis of CCT and GCT treated CdTe layers plotted using EDX results. Based on the EDX results as shown in Figure 5, deposition of Cd and Te elements were observed for all the CdTe layers explored without any traces of iodine. This might be due to no-iodine incorporation to the CdTe crystal lattice or very low levels of iodine incorporation which is undetectable by the EDX equipment. Further to the higher Cd to Te atomic ratio observed for the CdTe layer grown from the 0 ppm I-doped CdTe-bath, a 50:50 atomic composition ratio of Cd:Te was observed from the CdTe layer grown from bath containing 5 ppm I-doping. It is well documented in the literature that CdTe crystallinity is at its maximum at Cd/Te stoichiometry [27]. Further to this, a trend

relating the increase in the I-doping concentration in the CdTe-bath to an increase in the atomic concentration of Te as compared to Cd was also observable. This observation further confirms the hindrance of Cd and I deposition due to the possible formation of Cd-I complexes in aqueous solution [15,16]. These observations are in accordance with the summations made in Sections 3.1 and later in Sections 3.4 and 3.5.

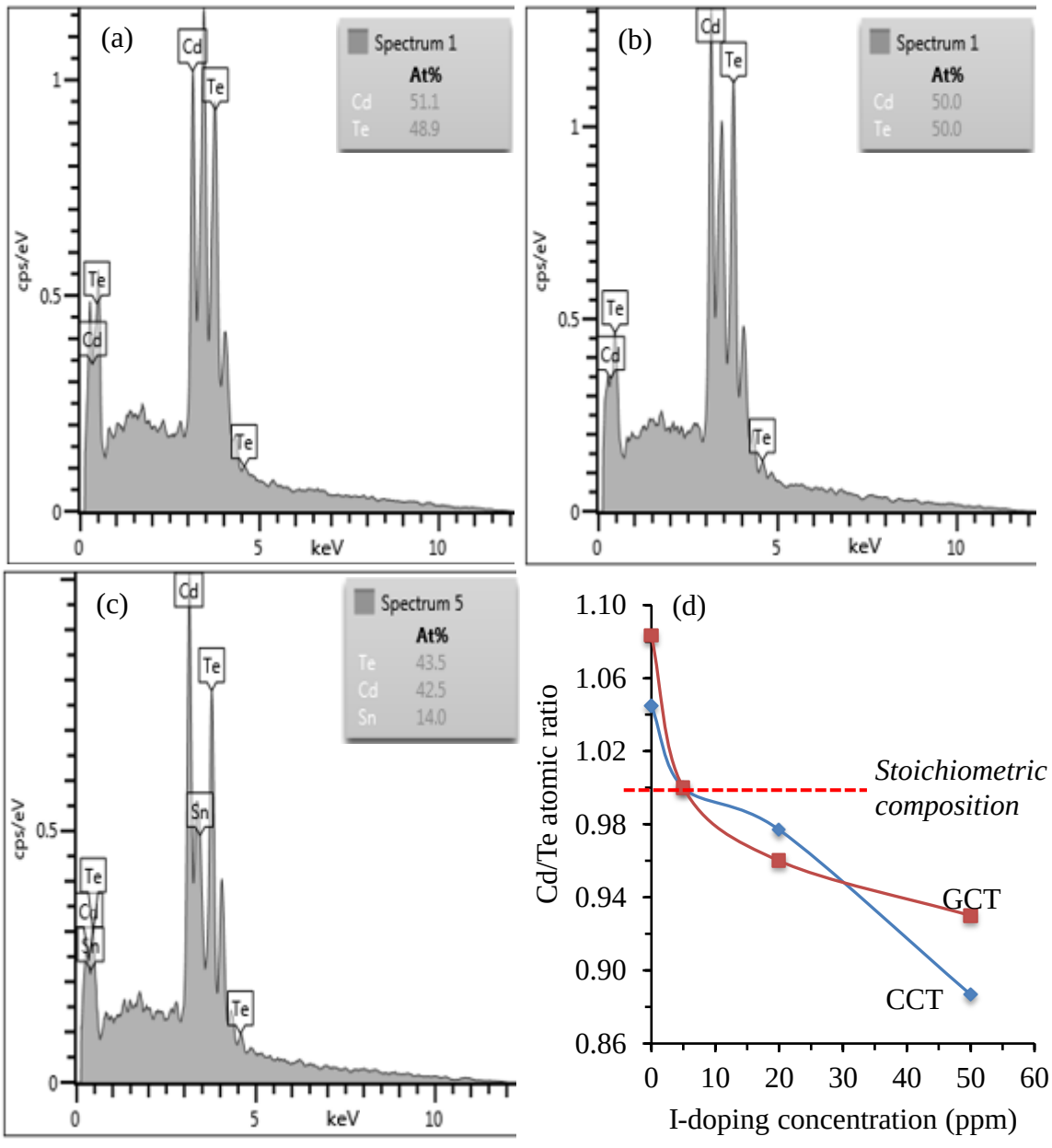

Figure 5: EDX spectra of CCT treated CdTe layers grown from CdTe bath containing ppm levels iodine at (a) 0, (b) 5 and (c) 20. While (d) show the Cd/Te atomic composition ratio of the CCT and GCT treated CdTe grown from baths containing varied I-doping concentration.

3.4 Photoelectrochemical (PEC) cell measurement

The use of PEC cell measurements instead of more robust electrical property measurements such as Hall Effect was due to the effect of the underlying glass/FTO conducting substrate on the electronic properties obtained. Figure 6 shows the graph of PEC cell measurement against varying I-doping concentration from 0 ppm to 200 ppm in CdTe:I bath. From observation, all the as-deposited CdTe:I layers at all the explored I-doping concentration shows *n*-type conductivity as it is well known that iodine along with other halogens are known as donors to CdTe due to the injection of excess electrons into the conduction band [28]. For both the CCT and GCT treated CdTe:I layers, the initial *n*-type conductivity were retained from the as-deposited CdTe:I for layers between 0 ppm and 10 ppm I-doping concentration while the transition to *p*-type conductivity was observed above 10 ppm I-doping concentration. It should be noted that the conduction type of a semiconductor material depends on the domination of factors such elemental composition, doping alteration due to annealing parameters, defect distribution amongst others [29,30]. In this case, at high I-concentration, Cd-deposition were hindered due to the Cd-I complex formation in aqueous solution. Therefore, the layers grown with a high concentration of iodine tend to be Te-rich and the heat treated materials become *p*-type in electrical condition.

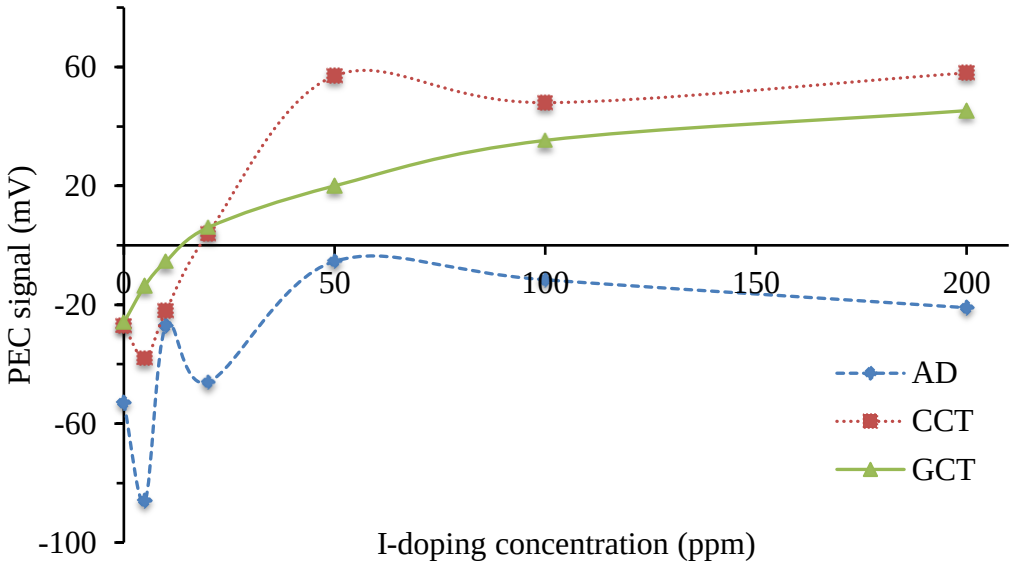

Figure 6: Photoelectrochemical cell measurement for AD, CCT and GCT CdTe:I layers.

3.5 DC properties analysis

The formation of Ohmic contacts with the CdTe:I was dependent on the conductivity type of the layers as discussed in PEC section. Gold (Au) was evaporated on *p*-type layers, while

indium (In) was evaporated on *n*-type layers. Figure 7 shows the graph of electrical conductivity against I-doping concentration in CdTe bath. It can be deduced from Figure 7 that the conductivity of Te-rich *p*-CdTe is lower than the Cd-rich *n*-CdTe layers. This observation is in accordance with the literature [31].

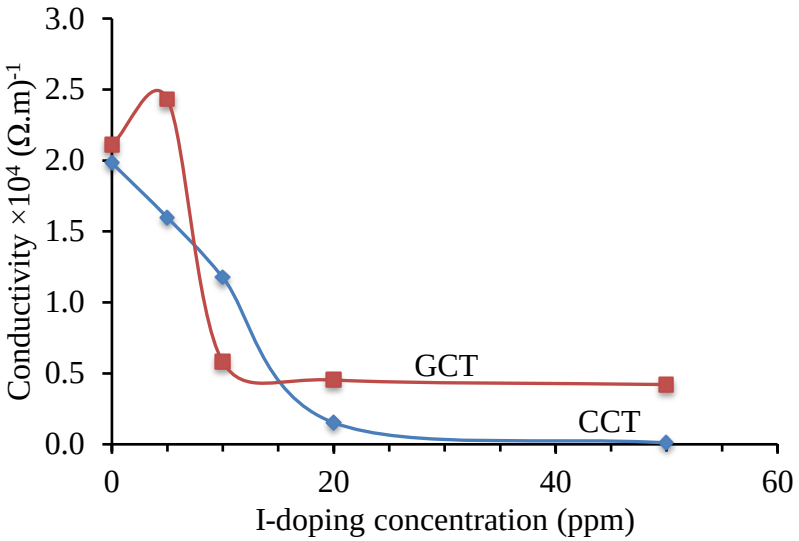

Figure 7: Graph of electrical conductivity against I-doping concentration in CdTe bath.

4 Conclusion

In this work, we have explored the effect of iodine doping in an aqueous CdTe electrolytic bath on the CdTe layer as it affects its structural, optical, morphological, compositional and selected electronic properties. An optimal I-doping concentration of 5 ppm in the electrolytic bath was observed under all material characterisations explored in this work due to the solubility limit achieved at 5 ppm I-doping and deterioration in material property afterwards. Although some literature shows improvement of CdTe properties with increased iodine doping [32] even in electrodeposition of CdTe:I from non-aqueous solution [19], this work demonstrate the limitation of property improvement of CdTe:I to 5 ppm using aqueous solution. The formation of various Cd-I complexes in aqueous solution severely slows down the deposition of Cd into the CdTe layer. Therefore, Te-rich layers with poor structural and electronic properties were formed at high I-concentrations. The incorporation of this work into PV device fabrication is ongoing.

Acknowledgement

The main author would like to acknowledge the Sheffield Hallam University, Tertiary Education Trust Fund (TETFund), Nigeria and the University of Ado Ekiti for their support.

References

1. F. V. Wald, Rev. Phys. Appliquée **12**, 277 (1977).

2. J. J. Loferski, J. Appl. Phys. **27**, 777 (1956).

3. W. Shockley and H. J. Queisser, J. Appl. Phys. **32**, 510 (1961).

4. A. A. Ojo and I. M. Dharmadasa, Mater. Chem. Phys. **180**, 14 (2016).

5. S. D. Sathaye and A. P. B. Sinha, Thin Solid Films **37**, 15 (1976).

6. A. Romeo, Growth and Characterization of High Efficiency CdTe/CdS Solar Cells, PhD Thesis, Swiss Federal Institute of Technology Zurich, 2002.

7. A. Bosio, N. Romeo, S. Mazzamuto, and V. Canevari, Prog. Cryst. Growth Charact. Mater. **52**, 247 (2006).

8. J. M. Burst, J. N. Duenow, D. S. Albin, E. Colegrove, M. O. Reese, J. A. Aguiar, C.-S. Jiang, M. K. Patel, M. M. Al-Jassim, D. Kuciauskas, S. Swain, T. Ablekim, K. G. Lynn, and W. K. Metzger, Nat. Energy **1**, 16015 (2016).

9. M. O. Reese, C. L. Perkins, J. M. Burst, S. Farrell, T. M. Barnes, S. W. Johnston, D. Kuciauskas, T. A. Gessert, and W. K. Metzger, J. Appl. Phys. **118**, 155305 (2015).

10. I. M. Dharmadasa, Prog. Cryst. Growth Charact. Mater. **36**, 249 (1998).

11. H. I. Salim, V. Patel, a. Abbas, J. M. Walls, and I. M. Dharmadasa, J. Mater. Sci. Mater. Electron. **26**, 3119 (2015).

12. P. Fernández, J. Optoelectron. Adv. Mater. **5**, 369 (2003).

13. I. M. Dharmadasa, Coatings **4**, 282 (2014).

14. N. B. Chaure, A. P. Samantilleke, R. P. Burton, J. Young, and I. M. Dharmadasa, Thin Solid Films **472**, 212 (2005).

15. R. Paterson, J. Anderson, S. S. Anderson, and Lutfullah, J. Chem. Soc. Faraday Trans. 1 Phys. Chem. Condens. Phases **73**, 1773 (1977).

16. R. Paterson and C. Devine, J. Chem. Soc. Faraday Trans. 1 Phys. Chem. Condens. Phases **76**, 1052 (1980).

17. A. A. Ojo and I. M. Dharmadasa, J. Mater. Sci. Mater. Electron. **28**, 14110 (2017).

18. I. M. Dharmadasa, P. Bingham, O. K. Echendu, H. I. Salim, T. Druffel, R. Dharmadasa, G. Sumanasekera, R. Dharmasena, M. B. Dergacheva, K. Mit, K. Urazov, L. Bowen, M. Walls, and A. Abbas, Coatings **4**, 380 (2014).

19. N. B. Chaure, A. P. Samantilleke, and I. M. Dharmadasa, Sol. Energy Mater. Sol. Cells **77**, 303 (2003).

20. A. Monshi, World J. Nano Sci. Eng. **02**, 154 (2012).

21. A. Bouraiou, M. S. Aida, O. Meglali, and N. Attaf, Curr. Appl. Phys. **11**, 1173 (2011).

22. J. Tauc, Mater. Res. Bull. **3**, 37 (1968).
23. C. Ferekides and J. Britt, Sol. Energy Mater. Sol. Cells **35**, 255 (1994).
24. A. A. Ojo and I. M. Dharmadasa, J. Electron. Mater. **45**, 5728 (2016).
25. M. A. Redwan, E. H. Aly, L. I. Soliman, A. A. El-Shazely, and H. A. Zayed, Vacuum **69**, 545 (2003).
26. H. Metin and R. Esen, Semicond. Sci. Technol. **18**, 647 (2003).
27. A. A. Ojo and I. M. Dharmadasa, Sol. Energy **136**, 10 (2016).
28. B. M. Basol, Sol. Cells **23**, 69 (1988).
29. B. M. Basol, Int. J. Sol. Energy **12**, 25 (1992).
30. T. M. Razykov, N. Amin, B. Ergashev, C. S. Ferekides, D. Y. Goswami, M. K. Hakkulov, K. M. Kouchkarov, K. Sopian, M. Y. Sulaiman, M. Alghoul, and H. S. Ullal, Appl. Sol. Energy **49**, 35 (2013).
31. P. J. Sellin, A. W. Dazvies, A. Lohstroh, M. E. Özsan, and J. Parkin, IEEE Trans. Nucl. Sci. **52**, 3074 (2005).
32. D. Brun-Le-Cunff, T. Baron, B. Daudin, S. Tatarenko, and B. Blanchard, Appl. Phys. Lett. **67**, 965 (1995).